Air-Stable Single-Source Precursors for the Synthesis of Chalcogenide Semiconductor Nanoparticles

M. Azad Malik,[†] Neerish Revaprasadu,[‡] and Paul O'Brien*[,§]

Department of Chemistry, Imperial College of Science, Technology and Medicine, South Kensington, London SW7 2AZ, United Kingdom, Department of Chemistry, University of Zululand, Private Bag X1001, Kwadlangezwa, 3886, and The Manchester Materials Science Centre and the Department of Chemistry, Manchester University, Oxford Road, Manchester M13 9PL, United Kingdom

Received August 22, 2000. Revised Manuscript Received October 16, 2000

Bis(hexylmethyldithio-/diselenocarbamato)cadmium(II)/zinc(II) ($M(E_2CNMe^nHex)_2$ [M = Zn, Cd; E = S, Se]) have been used as single-source precursors for the preparation of TOPO-capped CdS, CdSe, ZnS, and ZnSe nanoparticles. The precursors are stable for long periods of time and pyrolyse cleanly to give high yields of nanocrystals. The nanoparticles were of high quality, close to monodispersed, and showed quantum confinement with characteristic close to band edge luminescence in their emission spectra. The broad diffraction in the XRD pattern and diffuse diffraction rings of the SAED pattern are typical of nanometric size particles. The TEM micrographs showed well-defined, close to spherical particles and the lattice fringes in the HRTEM images confirmed the crystalline nature. The presence of a strong phosphorus peak in the EDAX spectra is indicative of TOPO or TOPE (E = S or Se) bound to the surface.

Introduction

Nanoparticles of semiconducting materials have been identified as materials with potential in a wide range of technological applications.[1−7] Much work has been done to evolve efficient routes for high-quality monodispersed quantum dots. Murray et al.[8] produced good quality CdSe nanoparticles passivated with tri-*n*-octylphosphine oxide (TOPO) using volatile metal alkyls and a chalcogen source. Alivisatos and co-workers[9] produced CdSe quantum dots by adapting Murray's method with the principle difference being the higher temperature (350 °C) of injection of the precursors. The formation of nanoparticles by both these methods was explained with an analogy to classical colloidal chemistry. Instantaneous nucleation after the injection of the reactants into the coordinating solvent at elevated temperatures is followed by controlled growth and annealing, in a formal sense consistent with Ostwald ripening. The use of single-source molecular precursors, as initially reported by Trindade and O'Brien,[10,11] has proven to be an efficient route to high quality, crystalline monodispersed nanoparticles of semiconducting materials. Air-sensitive alkylcadmium dithio- and diseleno carbamate complexes were used as precursors for the preparation of CdS and CdSe nanoparticles, with later work extending to the preparations to ZnS[12] and ZnSe[13] by using the zinc derivatives. Recently, air-stable (methylhexyldithio-/diselenocarbamato)cadmium/zinc complexes have been used as precursors for the deposition of thin films of II/VI chalcogenides by metal organic chemical vapor deposition (MOCVD)[14,15] and also for the growth of nanoparticles.[16] This paper reports the synthesis of TOPO-capped CdSe, CdS, ZnS, and ZnSe nanoparticles using the air-stable methylhexyldithio-/diselenocarbamato of cadmium/zinc precursors and their detailed characterization.

Experimental Section

Chemicals. Cadmium acetate, *N*-methylhexylamine, selenium, zinc acetate, zinc hydroxide, tri-*n*-octylphosphine (TOP), and tri-*n*-octylphosphine (TOPO) were purchased from Aldrich Chemical Co. Ltd. Carbon disulfide, 1,4-dioxane, methanol, and toluene were from BDH. The solvents used for air-sensitive chemistry were distilled, deoxygenated under a nitrogen flow, and stored over molecular sieves (type 4 Å, BDH) before use. TOPO was purified by vacuum distillation at ≈250

* To whom correspondence should be addressed.
[†] Imperial College of Science, Technology and Medicine.
[‡] University of Zululand.
[§] Manchester University.

(1) Henglein, A. *Chem. Rev.* **1989**, *89*, 1861.
(2) Steigerwald, M. L.; Brus, L. E. *Acc. Chem.* Res. **1990**, *23*, 183.
(3) Weller, H. *Angew. Chem., Int. Ed. Eng.* **1993**, *32*, 41.
(4) Weller, H. *Adv. Mater.* **1993**, *5*, 88.
(5) Hagfeldt, A.; Gratzel, M. *Chem. Rev.* **1995**, *95*, 49.
(6) Fendler, J. H.; Meldrum, F. C. *Adv. Mater.* **1995**, *95*, 607.
(7) Alivisatos, A. P. *Science* **1996**, *271*, 933.
(8) Murray, C. B.; Norris, D. J.; Bawendi, M. G. *J. Am. Chem. Soc.* **1993**, *115*, 8706.
(9) Bowen-Katari, J. E.; Alivisatos, A. P. *J. Phys. Chem.* **1994**, *98*, 4109.
(10) Trindade, T.; O'Brien, P. *Adv. Mater.* **1996**, *8*, 161.
(11) Trindade, T.; O'Brien, P. *Chem. Mater.* **1997**, *9*, 523.
(12) Revaprasadu, N.; Malik, M. A.; O'Brien, P.; Wakefield, G. *J. Mater. Res.* **1999**, *40* (8), 3237.
(13) Revaprasadu, N.; Malik, M. A.; O'Brien, P.; Zulu, M. M.; Wakefield, G. *J. Mater. Chem.* **1998**, *8* (8), 1885.
(14) Chunggaze, M.; McAleese, J.; O'Brien, P.; Otway, D. J. *Chem. Commun.* **1998**, 833.
(15) O'Brien, P.; Otway, D. J.; Walsh, J. R. *Adv. Mater. CVD* **1997**, *3*, 227.
(16) Ludolph, B.; Malik, M. A.; Revaprasadu, N. R.; O'Brien, P. *J. Chem. Soc. Chem. Commun.* **1998**, 1849.

10.1021/cm0011662 CCC: $20.00
Published on Web 02/07/2001

°C (0.1 Torr). The purity of TOPO was checked by ^{1}H NMR and melting point measurement (54 °C).

UV/Vis and IR Spectroscopy. A Philips PU 8710 spectrophotometer was used to carry out the optical measurements and the samples were placed in silica cuvettes (1-cm path length). The optical measurements were carried out using toluene as a reference.

The "optical band gap" (E_g) of the nanodispersed materials was determined by fitting the absorption edge data to a direct transition process. E_g was obtained by extrapolation after performing a linear regression on the absorption band edge data. (R^2 for the fit not less than 0.98). Infrared spectra were carried out using the Matteson Polaris FT-IR spectrometer as Nujol mulls.

Photoluminescence Spectroscopy. A Spex FluoroMax instrument with a xenon lamp (150 W) and a 152 P photomultiplier tube as a detector was used to measure the photoluminescence of the particles. Good spectra were obtained with the slits set at 2 nm and an integration time of 1 s. The samples were placed in quartz cuvettes (1-cm path length). The wavelength of excitation is indicated in the text and was shorter than the onset of absorption of the particular sample being studied.

X-ray Diffraction (XRD). X-ray diffraction patterns were measured using a Philips PW 1700 series automated powder diffractometer using Cu Kα radiation at 40 kV/40 mA with a secondary graphite crystal monochromator. Samples were supported on glass slides (5 cm). A concentrated suspension of the particles was slowly evaporated at room temperature onto a glass slide to obtain a sample for analysis. X-ray diffraction patterns on samples were performed using secondary graphite monochromated Cu Kα radiation (40 kV) on a Philips X'Pert Materials Research Diffractometer. Measurements were taken using a glancing angle incidence detector at an angle of 3°, for 2θ values over 20°−60° in steps of 0.04° with a count time of 1s.

Electron Microscopy. A Joel 2000 FX MK 1 operated at 200 kV electron microscope with an Oxford Instrument AN 10000 EDS Analyzer was used for the conventional TEM (transmission electron microscopy) images. Selected area electron diffraction (SAED) patterns were obtained using a JEOL 2000 FX MK2 electron microscope operated at 200 kV. The samples for TEM and SAED were prepared by placing a drop of a dilute solution of sample in toluene on a copper grid (400 mesh, agar). The excess solvent was wicked away with a paper tip and the sample allowed to dry completely at room temperature.

EDAX (energy-dispersive analytical X-ray) was performed on samples deposited by evaporation onto glass substrates using a JEOL JSM35CF scanning electron microscope. For the HRTEM images a drop of the dilute solution of sample was placed on a holey carbon film, left to evaporate, and then examined in a JEOL 4000EX TEM at 400 kV.

Synthesis. *CSe_2.* CSe_2 was prepared by a modification of the method of Henriksen and Kristiansen.[17] Carbon diselenide is a very toxic, evil-smelling liquid and extreme caution must be observed during preparation and manipulation. All experimental procedures must be carried out in a fume hood and under nitrogen. Approximately 10 g of selenium powder yielded ≈10 g of carbon diselenide. In general, three runs were carried out before purification and isolation of the product. The black residue from the reaction was filtered through neutral alumina and washed through with dichloromethane. The excess of CH_2Cl_2 was then removed from the filtrate by distillation (40 °C, atmospheric pressure), leaving a black oily residue that was vacuum-distilled (50 °C, 10^{-2} Torr) to give an intensely bright yellow liquid that was collected in a liquid nitrogen trap at −196 °C. Overall yield for the experiment was ≈30−35 g (yield 69% based on 30 g of selenium). The CSe_2 was placed in an airtight container and kept indefinitely at −25 °C.

Bis(hexylmethyldithio-/diselenocarbamato)cadmium(II)/zinc(II). Bis(hexylmethyldithio-/diselenocarbamato)cadmium(II)/zinc(II) were prepared essentialy by the literature methods.[18,19] Only a brief description of each preparation is given here.

$Cd(S_2CNMeHex)_2$. A mixture of $Cd(OH)_2 \cdot 2H_2O$ (8.43 g, 46.2 mmol), CS_2 (4.6 cm^3, 77.2 mmol), and *N*-methylhexylamine (11.6 cm^3, 76.3 mmol) in ethanol (50 cm^3) was heated at 70 °C for 1 h. The mixture was filtered to remove the solid impurities and the clear filtrate was evaporated under vacuum. The yellow solid product was recrystallized from chloroform at room temperature to give $Cd(S_2CNMeHex)_2$ (mp 74 °C; yield: 14.11 g, 28.6 mmol, 75%).

$Cd(Se_2CNMeHex)_2$. CSe_2 (4.13 g, 24.6 mmol) in 1,4-dioxane (50 cm^3) was slowly added via a dropping funnel to a solution of sodium hydroxide (1.00 g, 24.9 mmol) and *N*-methylhexylamine (3.7 cm^3, 24.6 mol) at −10 °C. The resultant orange solution was filtered and immediately added to a solution of cadmium acetate (3.23 g, 12.14 mmol) to give a yellow precipitate. The precipitate was then filtered and dried under vacuum. The crude product, a pale yellow solid, was recrystallized from chloroform at room temperature to give yellow $Cd(Se_2CNMeHex)_2$ (mp 80 °C; yield: 5.02 g, 7.4 mmol, 60%).

$Zn(S_2CNMeHex)_2$. The preparation of $Zn(S_2CNMeHex)_2$ was similar to that of $Cd(S_2CNMeHex)_2$; however, $Zn(OH)_2 \cdot 2H_2O$ (6.29 g, 46.5 mmol) was used instead of $Cd(OH)_2 \cdot 2H_2O$. The white solid product was recrystallized from chloroform at room temperature to give $Zn(S_2CNMeHex)_2$ (mp 68 °C; yield: 13.92 g, 31.2 mmol, 76%).

$Zn(Se_2CNMeHex)_2$. $Zn(Se_2CNMeHex)_2$ was synthesized in a manner similar to $Cd(Se_2CNMeHex)_2$, but zinc acetate (2.70 g, 12.30 mmol) was used instead of cadmium acetate. The crude product, a pale brown solid, was recrystallized from chloroform at room temperature to give $Zn(Se_2CNMeHex)_2$ (mp 72 °C; yield: 4.83 g, 7.6 mmol, 63%).

Method for the Preparation of Q-Dots. The TOPO-capped nanoparticles were synthesized by the injection of the appropriate single-source precursor (e.g., $Cd(S_2CNMeHex)_2$) dispersed in TOP into hot TOPO using standard Schlenck techniques. Typically, $Cd(S_2CNMeHex)_2$ (1.0 g) was dissolved in TOP (25 mL). This solution was then injected into hot TOPO (250 °C). A decrease in temperature of 20−30 °C was observed. The solution was then allowed to stabilize at 250 °C and heated for 30 min at this temperature. The solution was cooled to ≈70 °C, an excess of methanol added, and a flocculant precipitate formed. The solid was separated by centrifugation and redispersed in toluene. The toluene was removed under vacuum to give pale yellow TOPO-capped CdS nanoparticles. The particles were washed three times with methanol and redissolved in toluene.

The growth of the CdS and CdSe nanoparticles was monitored as a function of time by recording the optical absorption spectrum of an aliquot (2 mL), collected with a syringe, from the reactant solution. Size-selective precipitation was carried out on the first fraction of the CdS nanoparticles as described in the literature.[8] Briefly, this procedure involves the dropwise addition of methanol to the toluene solution containing the nanoparticles until the solution becomes turbid. The precipitate is separated by centrifugation to give a first fraction of nanoparticles. The second and subsequent fractions are obtained by repeating the same process with the supernatant.

Results and Discussion

$M(E_2CNMe^nHex)_2$ [M = Zn, Cd; E = S, Se] proved to be useful single-molecule precursors for the deposition of metal chalcogenides. These precursors are stable for periods of months, easy to synthesize, and pyrolyze cleanly to give good yields. We have previously inves-

(17) Henrikson, L.; Kristansen, E. S. S. *Int. J. Sulfur Chem. Part A* **1972**, *2*, 133.

(18) Motevalli, M.; O'Brien, P.; Walsh, J. R.; Watson, I. M. *Polyhedron* **1996**, *15*, 2801.

(19) Motevalli, M.; O'Brien, P.; Walsh, J. R.; Watson, I. M.; Henriksen, L. *J. Chem. Soc., Dalton Trans.* **1996**, 2491.

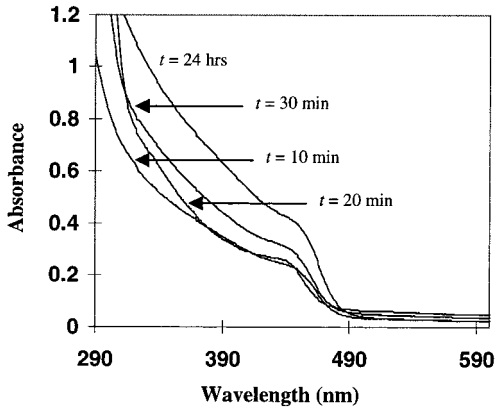

Figure 1. Optical spectra of CdS nanoparticles taken at different time intervals.

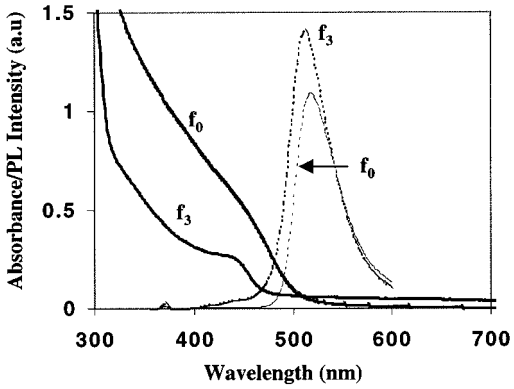

Figure 2. Optical absorption (solid line) and photoluminescence (dotted line) spectrum of fraction (f_0) and third fraction (f_3) of CdS nanoparticles.

tigated the effect of quite subtle changes in substituents at the nitrogen of a diseleno- or dithiocarbamate on the thermal decomposition of a metal complex as used in the preparation of chalcogenides.[20] The formation of stable ring structures might be expected to be enhanced, by having greater stabilizing substituents at the β-carbon to the nitrogen (e.g., bulkier alkyl groups), so that when the ring forms it may cleanly eliminate. Studies by GC-MS and EI-MS show the reason elemental selenium is deposited along with the metal selenide from the compounds such as $M(Se_2CNEt_2)_2$ [M = Zn or Cd] whereas $M(Se_2CNMe^nHex)_2$ [M = Zn, Cd] and $EtZnSe_2CNEt_2$ give clean deposits of metal selenides. The formation of selenium clusters Se_n, $n = 1-7$, is observed on the pyrolysis of diethyl derivatives whereas no selenium clusters were observed for methylhexyl or mixed alkyl derivatives.

Optical Properties of CdS and CdSe. TOPO-capped CdS and CdSe nanoparticles were synthesized at 250 °C using [Cd(S_2CNMeHex)$_2$] and [Cd(Se_2CNMeHex)$_2$] as the precursors. Particle growth was monitored by recording the optical spectra after 10 min, 20 min, 30 min, and 24 h. The optical spectra can be used to calculate an approximate band edge using the direct band gap method.[21] Macrocrystalline, hexagonal CdS has an optical band gap of 2.52 eV (490 nm) at room temperature.[21] The evolution of the absorption spectrum over time for CdS is shown in Figure 1. The band edges of the different samples are as follows: 2.64 eV (t = 10 min, 469 nm); 2.62 eV (t = 20 min, 473 nm); 2.60 eV (t = 30 min, 477 nm); and 2.50 eV (t = 24 h, 495 nm). The band edges for all the samples are blue-shifted in relation to the bulk material. The blue shift is associated with the CdS nanoparticles being smaller than the bulk exciton of CdS (a_B = 20 Å). The estimated particle size using the effective mass approximation (EMA) are 4.78 nm (t = 10 min), 4.96 nm (t = 20 min), 5.10 nm (t = 30 min), and 6.50 nm (t = 24 h) sample. The increase in particle size with time is consistent with an Ostwald ripening process. After injection of the precursor there is a critical size dependent on the concentration of the precursor. After the precursor supply is depleted, the size distribution broadens because the smaller, less stable particles collapse, forming larger particles. The optical spectrum for the (t = 24 h) sample is typical of a broad size distribution.

The size distribution of the fraction (t = 24 h) was narrowed by a selective precipitation procedure. Four fractions were obtained with varying particle sizes. The first fraction (f_1) has an absorption edge at 2.56 eV (484 nm), a blue shift in relation to the initial sample (f_0). The second fraction (f_2) and third fraction (f_3) exhibit further shifts at 2.63 eV (471 nm) and 2.67 eV (464 nm), respectively. The sharpness of the band edge increases from the initial fraction to the third fraction (Figure 2).

Bulk CdS is reported to have a broad emission with the emission maximum in the 500−700-nm region of the luminescence spectrum. The emission is due to recombination from surface defects (predominantly sulfur vacancies).[22] The photoluminescence spectra of f_0 and f_3 of CdS are red-shifted in relation to the corresponding absorption spectra, exhibiting an emission maximum at 521 and 514 nm ($\lambda_{exc.}$ = 480 nm), respectively. This Stokes shifted band edge luminescence has been attributed to emission from a "dark exciton".[23−26]

The optical absorption spectra of the CdSe measured over a time period are shown in Figure 3. The optical absorption edge 2.24 eV (t =10 min, 553 nm) shows a blue shift in relation to bulk CdSe, 1.73 eV (716 nm). The first excitonic peak at ≈530 nm for (t =10 min) is due to the first electronic transition (1s−1s) occurring in the CdSe nanoparticles.[9,27] The second, less defined feature at ≈433 nm could be assigned to the higher spin−orbit component of the 1s−1s transition.[27] The band edges of the subsequent samples are as follows: 2.0 eV (t = 20 min, 619 nm); 1.97 eV (30 min, 629 nm); and 1.95 eV (t = 24 h, 635 nm,). The first excitonic peak observed in the (t = 10 min) is less pronounced in the latter samples. The calculated diameter of the latter samples are as follows: 5.88 nm (t = 20 min); 6.16 nm (t = 20 min); and 6.38 nm (t = 24 h).

(20) Chunggaze, M.; Malik, M. A.; O'Brien, P. *J. Mater. Chem.* **1999**, *9* (10), 2433.
(21) Pankove, J. I. *Optical Processes in Semiconductors*; Dover Publications: New York, 1970.
(22) Chestnoy, N.; Harris, T. D.; Hull, R.; Brus, L. E. *J. Phys. Chem.* **1986**, *90*, 3393.
(23) Efros, A. L.; Rosen, M.; Kuno, M.; Nirmal, M.; Norris, D. J.; Bawendi, M. G. *Phys. Rev.* **1996**, *B54*, 4843.
(24) Nirmal, M.; Norris, D. J.; Kuno, M.; Bawendi, M. G.; Efros, A. L.; Rosen M. *Phys. Rev. Lett.* **1995**, *75*, 3728.
(25) Nirmal, M.; Dabbousi, B. O.; Bawendi, M. G.; Macklin, J. J.; Trautman, J. K.; Harris, T. D.; Brus, L. E *Nature* **1996**, *383*, 802.
(26) Banin, U.; Bruchez, M.; Alivisatos, A. P.; Ha, T.; Weiss, S.; Chemia, D. S. *J. Chem. Phys.* **1999**, *110* (2), 1195.
(27) Bawendi, M. G.; Steigerwald, M. L.; Brus, L. E. *Annu. Rev. Phys. Chem.* **1990**, *41*, 477.

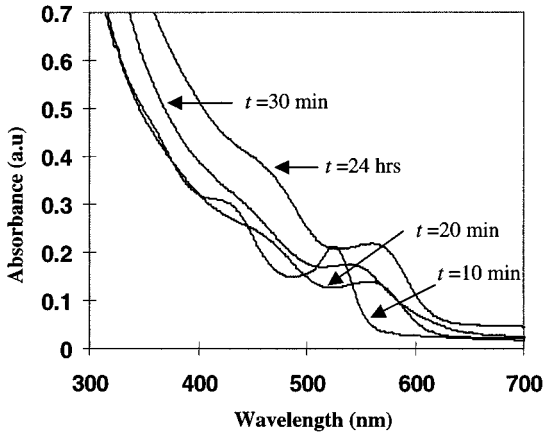

Figure 3. Optical spectra of CdSe nanoparticles taken at different time intervals.

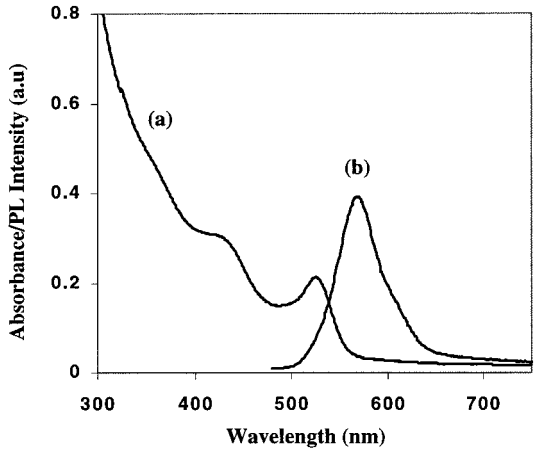

Figure 4. (a) Optical absorption spectrum and (b) photoluminescence spectrum of CdSe nanoparticles (t = 10 min).

The photoluminescence spectrum of CdSe in the reaction mixture of bis(hexylmethyldiselenocarbamato)-cadmium(II) in TOPO after 10 min shows a red shift in relation to the corresponding optical spectrum (Figure 4). The photoluminescence peak is narrow with an emission maximum at 575 nm ($\lambda_{exc.}$= 480 nm). The Stokes shift of 13 nm in relation to the band edge is due to the relaxation of the excited electron into a dark state, followed by recombination to the ground state as observed previously for TOPO-capped CdSe nanoparticles.[23−25] There is no evidence of any deep-trap emission.

Both the TOPO-capped ZnS and ZnSe nanoparticles show blue shifts in their absorption band edges. The band edge of ZnS, 318 nm (3.90 eV), shows a blue shift of 22 nm in relation to bulk ZnS, 340 nm (3.65 eV) (Figure 5). The spectrum shows no visible excitonic features; such bands are prominent in the absorption spectra[8,26] of CdS, CdSe, and ZnSe. The absorption spectrum of ZnSe shows an excitonic shoulder at 348 nm with the band edge at 421 nm (2.91 eV), a considerably larger blue shift from the bulk material (480 nm, 2.58 eV) (Figure 6). The photoluminescence spectrum of ZnS shows a broad emission due to the broad size of particles with the emission maximum at 404 nm. This large red shift as observed previously could be attributed to recombination from surface traps[29,30] or the concentration of nanoparticles in the solution was too high, which caused re-emission. ZnSe shows narrow band

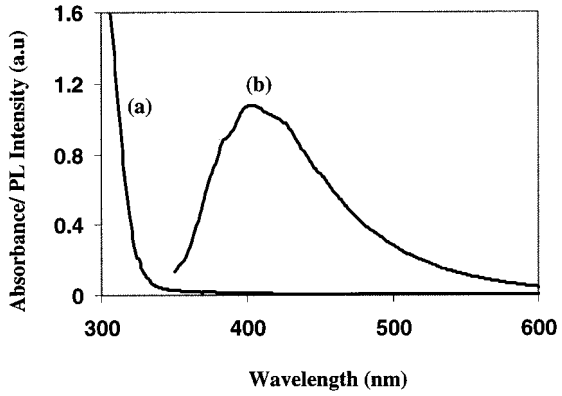

Figure 5. (a) Optical absorption spectrum and (b) photoluminescence spectrum of ZnS nanoparticles.

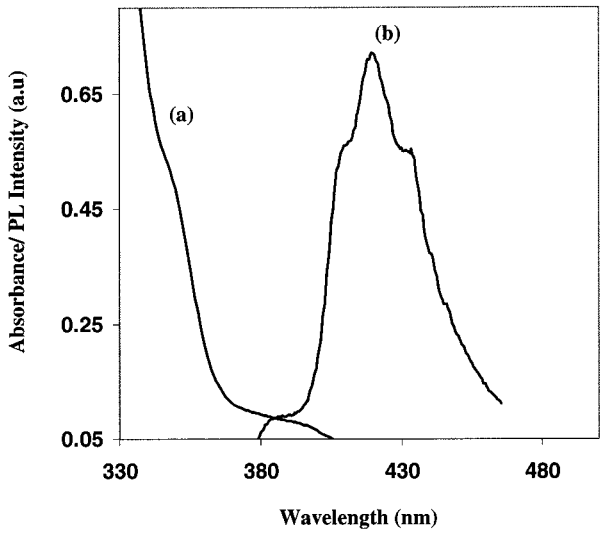

Figure 6. (a) Optical absorption spectrum and (b) photoluminescence spectrum of ZnSe nanoparticles.

edge luminescence, with an emission maximum at 428 nm.

Structural Characteristics. CdS and CdSe nanoparticles can exist as either the cubic or the hexagonal phase. However, the relatively small size of these particles makes it difficult to assign with complete certainty the exclusive existence of either phase. The existence of a mixture of cubic and hexagonal phase with the predominance of one over the other is a possibility as reported by Bawendi et al.[31] for CdSe nanoparticles.The X-ray diffraction pattern of both the CdS and CdSe nanoparticles synthesized in this work are consistent with predominantly the hexagonal phase. The CdS diffraction pattern (Figure 7) shows broad peaks typical of particles in the nanosize regime. The (110), (103), and (112) planes of wurtzite CdS are clearly distinguishable in the pattern. Table 1 shows the XRD and SAED data for CdS. The SAED pattern consists of broad diffuse rings, which are indicative of the small size of the particles. The diffraction rings can be

(28) Peng, X. G.; Wickham, J.; Alivisatos, A. P. *J. Am. Chem. Soc.* **1998**, *120*, 5343.
(29) Sooklal, K.; Cullum, B. S.; Angel, S. M.; Murphy, C. J. *J. Phys. Chem.* **1996**, *100*, 4551.
(30) Yang, Y.; Huang, J.; Liu, S.; Shen, J. *J. Mater. Chem.* **1997**, *7* (1), 131.
(31) Bawendi, M. G.; Kortan, A. R.; Steigerwald, M. L.; Brus, L. E. *J. Chem. Phys.* **1989**, *91*, 7282.

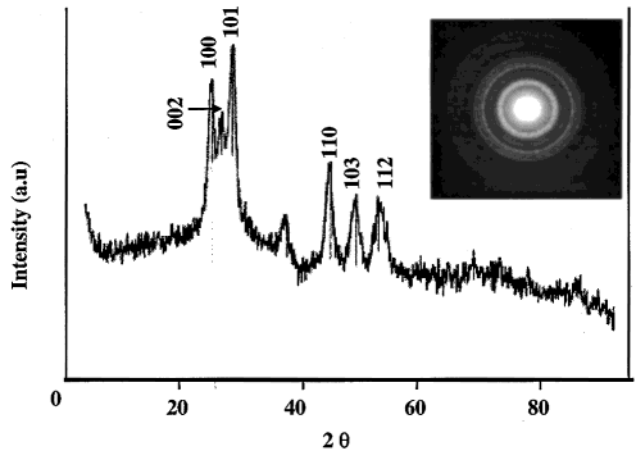

Figure 7. X-ray diffraction and SAED partterns of CdSe nanoparticles.

Table 1. XRD and SAED Data for CdS

XRD data			SAED data	
d(exp.)/Å	*d*(lit.)/Å	*hkl*	*d*(exp.)/Å	*hkl*
3.55	3.57	100	3.60	100
3.33	3.36	002		
3.16	3.16	101	3.20	101
2.06	2.07	110		
1.90	1.90	103	1.87	103
1.76	1.76	112	1.75	112

Table 2. XRD and SAED Data for CdSe

XRD data			SAED data	
d(exp.)/Å	*d*(lit.)/Å	*hkl*	*d*(exp.)/Å	*hkl*
3.70−3.30	3.72	100		
	3.50	002		
	3.29	101		
2.13	2.15	110	2.17	110
1.84	1.83	112	1.85	112
1.48	1.38	211		

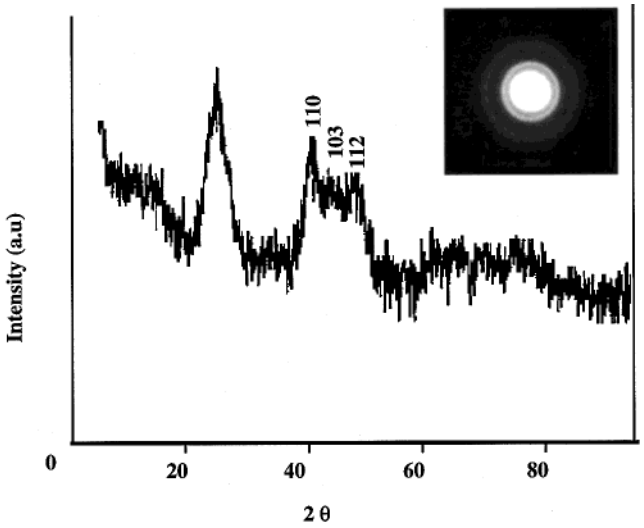

Figure 8. X-ray diffraction and SAED patterns of CdSe nanoparticles.

indexed, to the (100), (102), (103) and (112) planes, confirming the wurtzite phase. The diffraction pattern (Figure 8) of nanocrystalline CdSe also shows features typical of nanodimensional particles. The (110), (103), and (112) planes of wurtzite CdSe are not well-defined, appearing as a broad peak, indicating the small size of particles. The peaks along (002), (100), and (101) planes

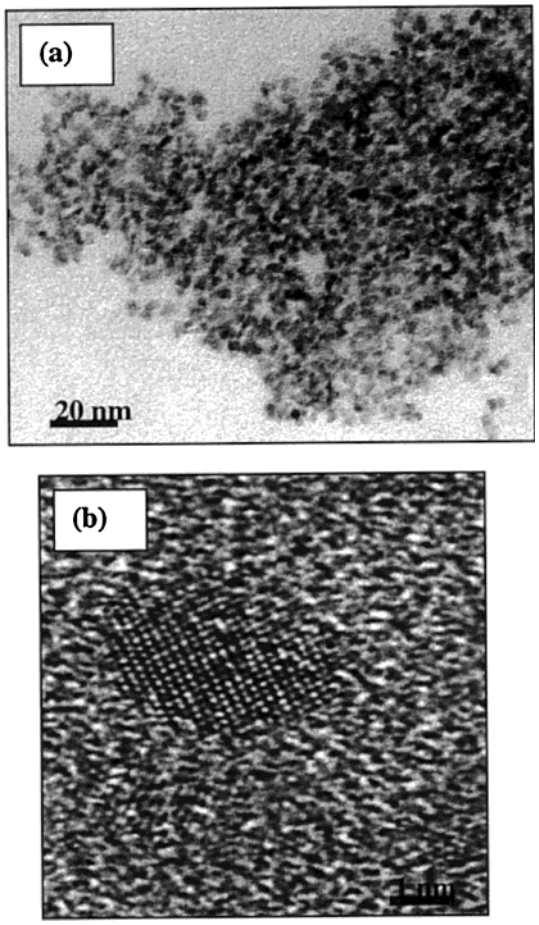

Figure 9. (a) TEM image of CdS (t = 10 min) and (b) HRTEM image showing a single quantum dot (approximate diameter = 5 nm).

shown in the hexagonal CdS diffraction pattern are not visible in the CdSe patterns due to broadening of the peak in the region d$\theta \cong 20°-25°$. The indexing of the diffuse rings of the SAED pattern confirms the (110) and (112) planes of the wurtzite phase.

The TEM image (Figure 9a) of CdS nanoparticles shows spherical particles that are ≈51.2 Å in size with a standard deviation of ±2.8 Å, a narrow size distribution.The crystallinity of the material is shown by clear lattice fringes of a single CdS dot in a HRTEM image (Figure 9b).

The particle size as determined from the TEM images of CdSe are as follows: 46.4 ± 6 Å (t = 10 min); 47.8 ± 4.7 Å (t = 20 min); 50.6 ± 4.4 Å (t = 30 min); and 51.8 ± 5.3 Å (t = 24 h). The TEM images and particle size distribution for CdSe (t = 10 min and t = 24 h) are shown in Figure 10. The TEM images for both samples show well-defined, monodispersed, spherical TOPO-capped CdSe particles. The increase in the average diameter in the latter sample is consistent with the observed red shift in the band edge from 10 min to 24 h. However, the difference in the particle size (≈5.4 Å) between the two samples as observed by TEM is not as large as that calculated using the effective mass approximation (EMA) model, which suggests a difference of ≈18.6 Å. The diameter of the particles as calculated by the EMA model is expected to be higher than that observed by TEM because the parameters used in the EMA model are those of the bulk material. The calcula-

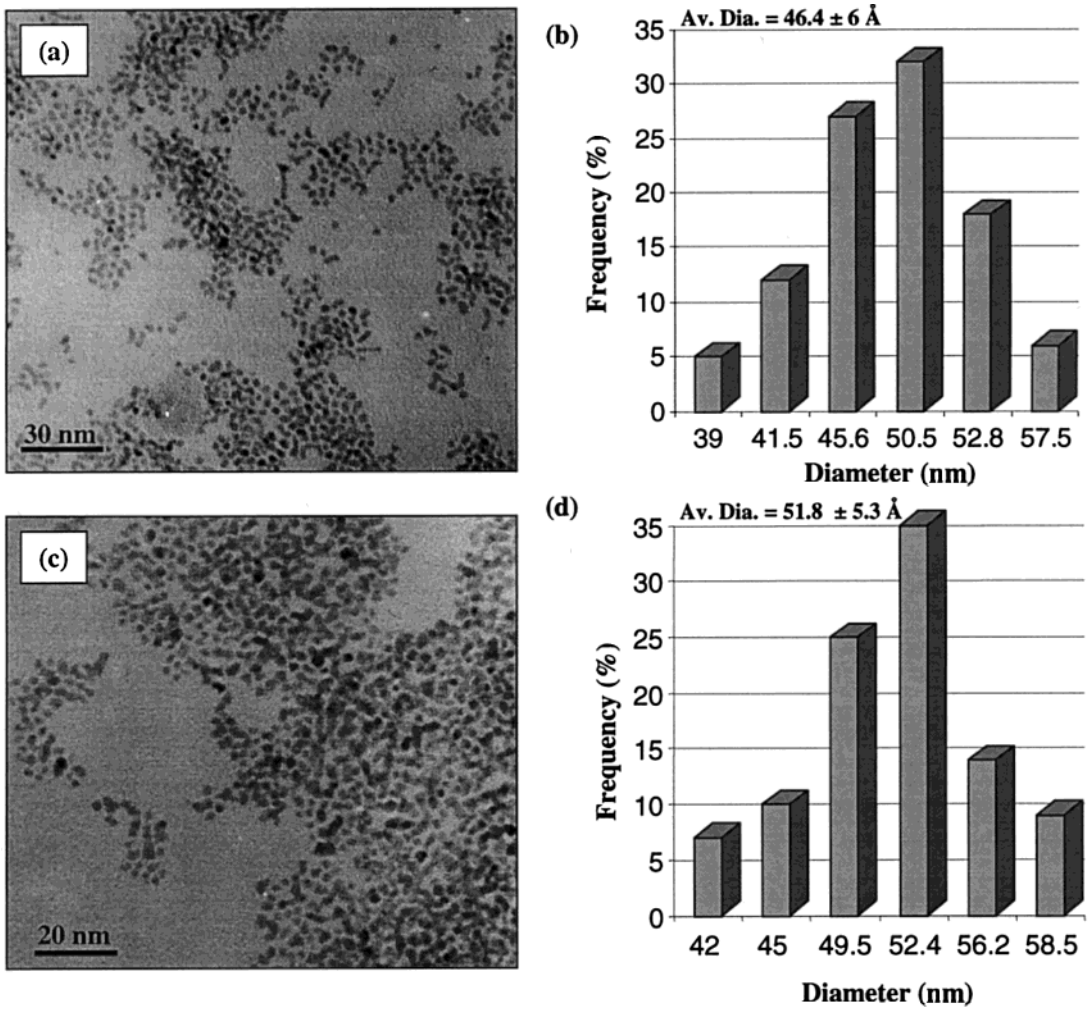

Figure 10. CdSe nanoparticles: (a) TEM image of (t = 10 min) and (b) corresponding particle size distribution; (c) TEM of (t = 24 h) and (d) corresponding particle size distribution.

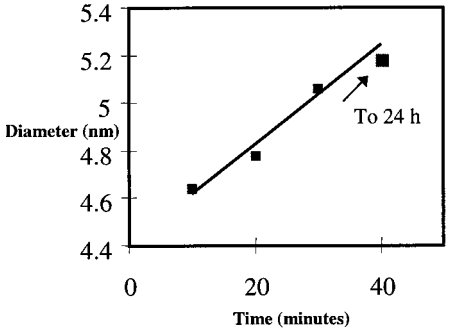

Figure 11. Plot of average of CdSe nanoparticles as a function of time.

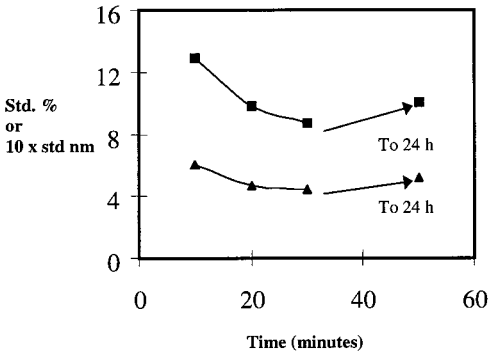

Figure 12. Plot of standard deviation of CdSe particle size as a function of time.

tions for the 24-h sample are consistent with the above observations; however, the particle size of the 10-min sample as observed by TEM is higher than that predicted by the EMA model. Trindade et al.[9] made similar observations, which were attributed to the overestimation of the particle size due to a loss of contrast in the TEM because of the presence of the passivating layer.

A plot of the diameter of CdSe nanoparticles as observed in the TEM as a function of time is shown in Figure 11. The graph indicates the steady increase in particle size from 10 min to 24 h. Figure 12 is a plot of the standard deviation (%) as a function of time. From this graph there is a decrease in the standard deviation from ±12.93% (6 Å) to ±8.69% (4.4 Å) from the (t = 10 min) to the (t = 30 min) sample, indicating a narrowing of the particle size distribution. The particle size distribution increases after 24 h (σ = ±10.13%). A similar trend has been reported previously for CdSe nanoparticles by Alivisatos,[26] who explained the phenomena on the basis of classical colloidal chemistry. The initial decrease in size distribution occurs when the CdSe nanoparticles are larger than the critical size at equilibrium, resulting in the faster growth of the smaller particles in relation to that of the larger particles. The size distribution broadens again when the precursor

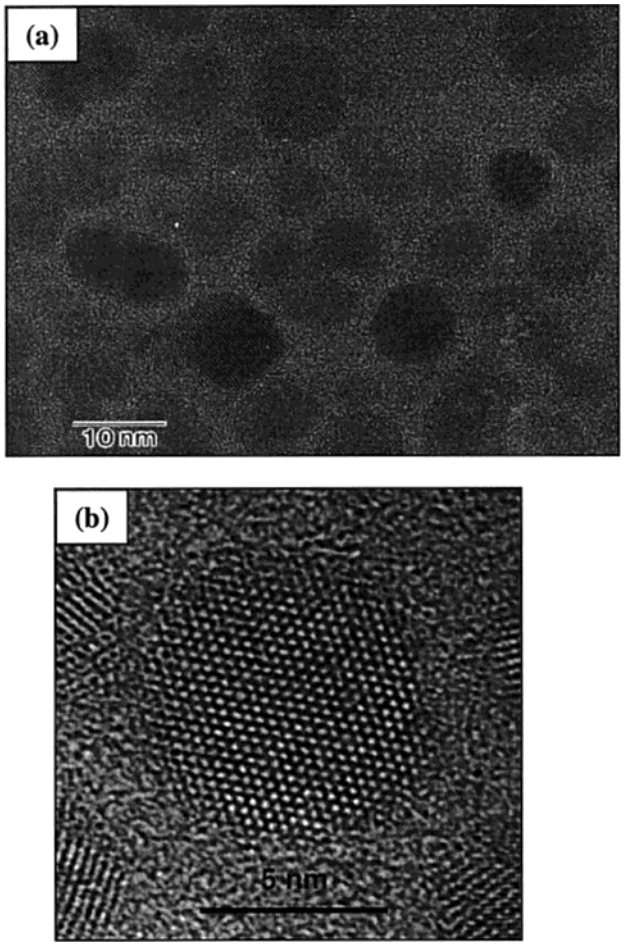

Figure 13. (a) HRTEM image of an array of CdSe nanoparticles; (b) single quantum dot of CdSe (approximate diameter = 5 nm).

supply is depleted. The smaller nanoparticles collapse, while the larger particles continue to grow.

The HRTEM image (Figure 13a) shows an array of CdSe nanoparticles. The lattice fringes are clearly visible, confirming their crystallinity. The particles visible in the image show the presence of stacking faults. This defect feature is very prominent in the image of a single quantum dot of CdSe (Figure 13b) and has been observed previously for CdSe nanoparticles.[8] The observed lattice spacing of 3.5 Å in the CdSe quantum dot (approximate diameter = 5 nm) corresponds to the (101) plane of hexagonal CdSe.

The EDAX spectrums for CdSe and CdS show the presence of cadmium and the corresponding chalcogen. There is a very strong phosphorus peak confirming the passivation of the particles by TOPO. The surface morphology of the TOPO-capped nanoparticles was investigated by IR spectroscopy. TOPO absorbs strongly at 1466 and 1146 cm^{-1}. The position of the (ν_{sym}, P=O, 1140−1320 cm^{-1}) depends on attached groups.[32] A shift of 20 cm^{-1} to lower wavenumbers for the (ν_{sym}, P=O) band has been reported by others for TOPO bound to the CdSe;[9] however, in this work there is a shift of 5 cm^{-1} for CdSe, with no visible change observed for CdS. The band of TOPO at 1466 cm^{-1} was observed for the CdSe (1465 cm^{-1}) and CdS (1468 cm^{-1}). These results are in agreement with those reported by Trindade et al.,[11] who also reported little change in the (ν_{sym}, P=O) band. The difference in findings from those of Alivisatos et al.[9] was explained by considering the surface composition of nanoparticles. There is an excess of Me_2Cd in the conventional route to CdSe, whereas the use of single-molecule precursors results in a 1:4 ratio of Cd/E (i.e., excess of chalcogenide in relation to metal) as is the case in this work. This could be the reason for a different surface composition, which in turn affects the (ν_{sym}, P=O) mode in the IR spectra.

TEM images of ZnS and ZnSe show nanosized particles with average diameters of 5.79 nm ± 5% (Figure 14a) and 4.98 nm ± 8.90% (Figure 15a), respectively. The HRTEM image of ZnS shows visible lattice fringes, indicating their crystallinity (Figure 14b). The indexing of the SAED pattern showed the peaks along (110), (103), and (112) planes, which correspond to the hexagonal phase of ZnS (Figure 14d). The XRD pattern of ZnSe shows broad peaks in the $d\theta \cong 25°-35°$ and $d\theta \cong 42°-52°$, which indicates that the particles are very small and/or poorly crystalline. The small size and poor crystallinity is confirmed by the diffuse rings of the SAED pattern (Figure 15c), making phase assignment difficult. The EDAX spectrum of both ZnS and ZnSe show the presence of zinc and the expected chalcogen.

Conclusions

The single-source route was used for the preparation of TOPO-capped CdS, CdSe, ZnS, and ZnSe nanoparticles by the thermolysis of $M(E_2CNMe^nHex)_2$ [M = Zn, Cd; E = S, Se]. The CdS and CdSe nanoparticles were high quality and monodispersed and clearly showed quantum confinement. The growth of both the CdS and CdSe nanoparticles was monitored over a period of time (from 10 min to 24 h) by UV/vis spectroscopy after the injection of the precursor (solution in TOP) into TOPO. A steady increase in particle size as a function of time was observed. The monitored particle size distribution for CdSe is consistent with previous findings for CdSe and can be explained by analogy to classical colloidal kinetics. The first fraction of the CdS nanoparticles size fractionated had a narrower size distribution clearly evident in the latter fractions. Both the CdS and CdSe nanoparticles show characteristic band edge luminescence in their emission spectra. In the case of CdS there is no evidence of any deep trap emission, confirming efficient passivation of the surface by TOPO. For CdSe, an emission peak at ≈750 nm in the PL spectrum (t = 24-h sample) is indicative of luminescence from surface traps. Both the TOPO-capped ZnS and ZnSe nanoparticles show blue shifts in their absorption band edges. The PL spectrum of ZnS nanoparticles shows a broad emission peak attributed to emission from surface traps, whereas the PL spectrum of the ZnSe nanoparticles is at the band edge.

The broad diffraction peaks of the XRD pattern and diffuse diffraction rings of the SAED pattern of both CdS and CdSe showed the materials to be of the nanometric size regime with a predominantly hexagonal phase. The TEM micrographs showed well-defined, close to spherical particles of CdS and CdSe particles. Nanometric particles are visible in the TEM images of both ZnS and

(32) Colthup, N. B.; Daly, L. H.; Wiberley, S. E. *Introduction to Infrared and Raman Spectroscopy*, 3rd ed.; Academic Press Inc.: San Diego, 1990; p 364.

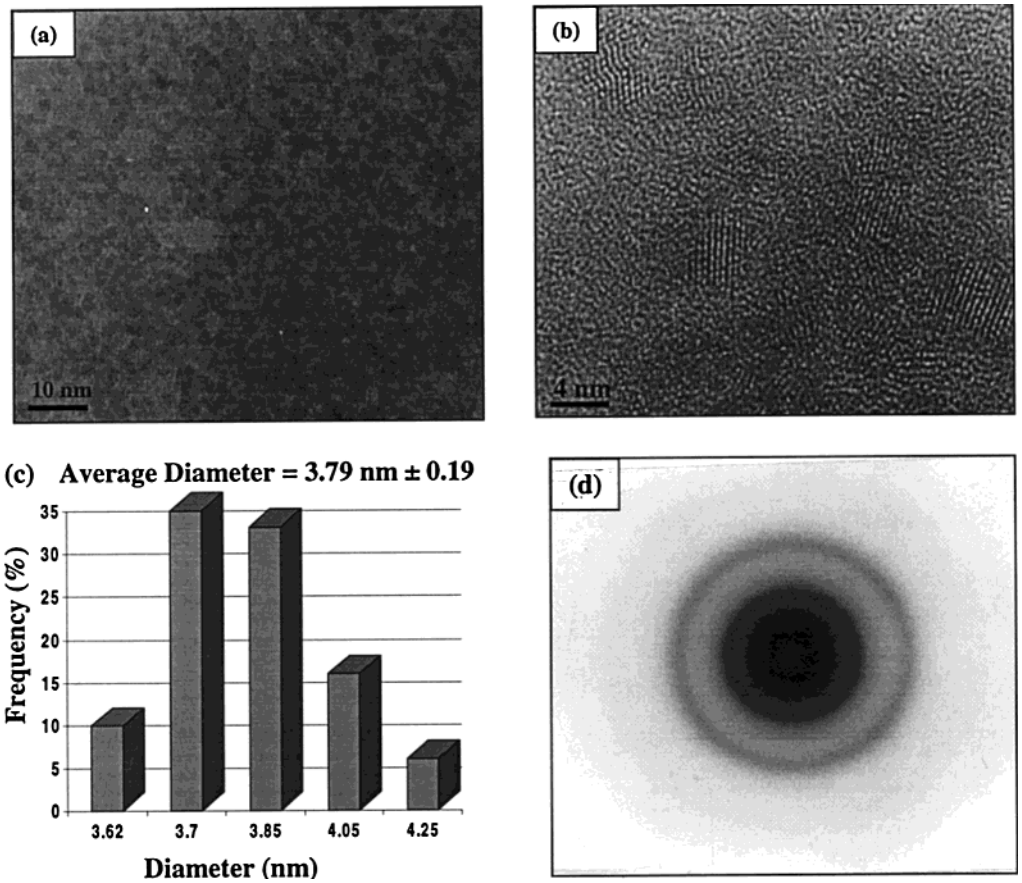

Figure 14. ZnS nanoparticles: (a) TEM image; (b) HRTEM image showing lattice fringes; (c) particle size distribution; and (d) SAED pattern.

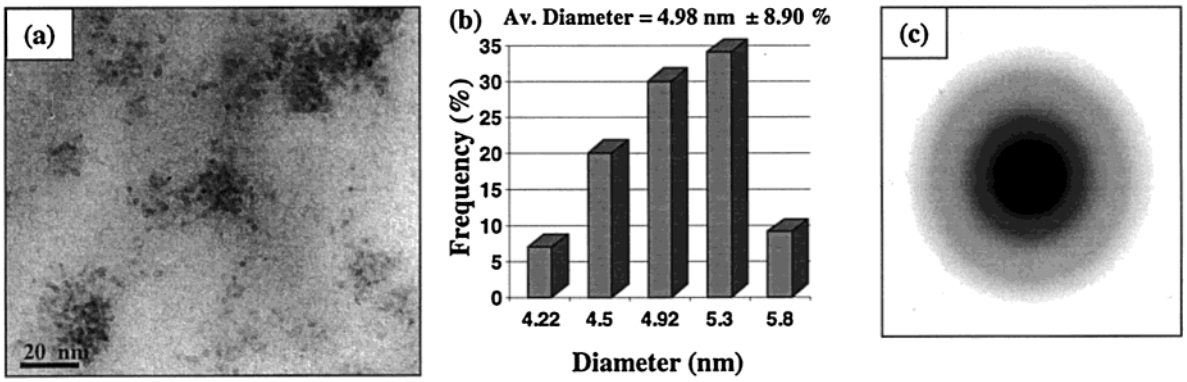

Figure 15. ZnSe nanoparticles: (a) TEM image; (b) particle size distribution; and (c) SAED pattern.

ZnSe. The SAED pattern of ZnS suggests that the hexagonal phase is dominant, with the crystallinity confirmed by the lattice fringes in the HRTEM image

Acknowledgment. We thank the Royal Society and the National Research Foundation (NRF) for support to N.R. and a program of collaboration between UZULU and ICSTM. P.O.B thanks the EPSRC for grants. P.O.B is the Sumitomo/STS visiting Professor of Materials Chemistry at ICSTM.

CM0011662